

# Studies of systematic uncertainties in the estimation of the monocular aperture of the HiRes experiment

R.U. Abbasi<sup>a</sup>, T. Abu-Zayyad<sup>a</sup>, J.F. Amman<sup>b</sup>, G. Archbold<sup>a</sup>,  
 K. Belov<sup>a</sup>, J.W. Belz<sup>c</sup>, S.Y. Ben Zvi<sup>d</sup>, D.R. Bergman<sup>e</sup>,  
 S.A. Blake<sup>a</sup>, O. Brusova<sup>a</sup>, G.W. Burt<sup>a</sup>, Z. Cao<sup>a</sup>,  
 B.C. Connolly<sup>d</sup>, W. Deng<sup>a</sup>, Y. Fedorova<sup>a</sup>, C.B. Finley<sup>d</sup>,  
 R.C. Gray<sup>a</sup>, W.F. Hanlon<sup>a</sup>, C.M. Hoffman<sup>b</sup>, G.A. Hughes<sup>e</sup>,  
 M.H. Holzscheiter<sup>b</sup>, P. Hüntemeyer<sup>a</sup>, B.F. Jones<sup>a</sup>, C.C.H. Jui<sup>a</sup>,  
 K. Kim<sup>a</sup>, M.A. Kirn<sup>c</sup>, E.C. Loh<sup>a</sup>, M.M. Maestas<sup>a</sup>,  
 N. Manago<sup>g</sup>, L.J. Marek<sup>b</sup>, K. Martens<sup>a</sup>, J.A.J. Matthews<sup>f</sup>,  
 J.N. Matthews<sup>a</sup>, S.A. Moore<sup>a</sup>, A. O'Neill<sup>d</sup>, C.A. Painter<sup>b</sup>,  
 L. Perera<sup>e</sup>, K. Reil<sup>a</sup>, R. Riehle<sup>a</sup>, M. Roberts<sup>f</sup>, D. Rodriguez<sup>a</sup>,  
 M. Sasaki<sup>g</sup>, S.R. Schnetzer<sup>e</sup>, L.M. Scott<sup>e</sup>, G. Sinnis<sup>b</sup>,  
 J.D. Smith<sup>a</sup>, P. Sokolsky<sup>a</sup>, C. Song<sup>d</sup>, R.W. Springer<sup>a</sup>,  
 B.T. Stokes<sup>a</sup>, J.R. Thomas<sup>a</sup>, S.B. Thomas<sup>a</sup>, G.B. Thomson<sup>e</sup>,  
 D. Tupa<sup>b</sup>, S. Westerhoff<sup>d</sup>, L.R. Wiencke<sup>a</sup>, A. Zech<sup>e,h,1</sup>,  
 X. Zhang<sup>d</sup>

<sup>a</sup>*University of Utah, Department of Physics and High Energy Astrophysics Institute, Salt Lake City, Utah, USA*

<sup>b</sup>*Los Alamos National Laboratory, Los Alamos, NM, USA*

<sup>c</sup>*University of Montana, Department of Physics and Astronomy, Missoula, Montana, USA*

<sup>d</sup>*Columbia University, Department of Physics and Nevis Laboratory, New York, New York, USA*

<sup>e</sup>*Rutgers - The State University of New Jersey, Department of Physics and Astronomy, Piscataway, New Jersey, USA*

<sup>f</sup>*University of New Mexico, Department of Physics and Astronomy, Albuquerque, New Mexico, USA*

<sup>g</sup>*University of Tokyo, Institute for Cosmic Ray Research, Kashiwa, Japan*

<sup>h</sup>*LUTH, Observatoire de Paris, Meudon, France*

The High Resolution Fly's Eye Collaboration

---

**Abstract**

We have studied several sources of systematic uncertainty in calculating the aperture of the High Resolution Fly’s Eye experiment (HiRes) in monocular mode, primarily as they affect the HiRes-II site. The energy dependent aperture is determined with detailed Monte Carlo simulations of the air showers and the detector response. We have studied the effects of changes to the input energy spectrum and composition used in the simulation. A realistic shape of the input spectrum is used in our analysis in order to avoid biases in the aperture estimate due to the limited detector resolution. We have examined the effect of exchanging our input spectrum with a simple  $E^{-3}$  power law in the “ankle” region. Uncertainties in the input composition are shown to be significant for energies below  $\sim 10^{18}$  eV for data from the HiRes-II detector. Another source of uncertainties is the choice of the hadronic interaction model in the air shower generator. We compare the aperture estimate for two different models: QGSJet01 and SIBYLL 2.1. We also describe the implications of employing an atmospheric database with hourly measurements of the aerosol component, instead of using an average as has been used in our previously published measurements of the monocular spectra.

*Key words:*

cosmic rays, UHECR flux, energy spectrum, Monte Carlo simulation

*PACS:* 98.70.Sa, 96.40.Pq, 05.10.Ln, 07.05.Tp, 24.10.Lx

---

**1 Introduction**

The High Resolution Fly’s Eye experiment consists of two air fluorescence detectors (“HiRes-I” and “HiRes-II”) located in the desert of Utah. HiRes observes ultra-high energy cosmic rays indirectly through extensive air showers, i.e. cascades of secondary charged particles, which are caused by interactions of the primary cosmic ray particles with the earth’s atmosphere. In the wake of the air shower, excited nitrogen molecules emit fluorescence light in the ultraviolet, which is collected by mirrors and projected onto clusters of photomultiplier tubes. Detailed descriptions of the detectors can be found in [1] and [2].

The HiRes experiment aims at measuring the arrival directions, composition, and flux of the most energetic cosmic rays. The two detectors allow stereoscopic observation of air showers, which yields the best resolution in shower geometry and cosmic ray energy. An advantage of data analysis in monocular

---

<sup>1</sup> To whom correspondence should be addressed. E-mail: [Andreas.Zech@obspm.fr](mailto:Andreas.Zech@obspm.fr)

mode, i.e. separate analyses of the data from each of the two detectors, lies in the higher statistics that can be achieved at the high energy end due to the longer lifetime of the HiRes-I detector, which started operation two years before HiRes-II, in 1997. Monocular analysis also allows an extension of the observed energy range down to energies as low as  $\sim 10^{17}$  eV due to the larger elevation coverage and better time resolution of the HiRes-II detector, and also due to the necessity of triggering only one detector. The differential flux or “energy spectrum” observed in monocular mode by HiRes shows a hardening in the flux at around  $10^{18.5}$  eV, known as the “ankle”, and a suppression of the flux near  $10^{19.8}$  eV, at the expected energy of the GZK flux suppression [3,4]. These results have been published in [5].

The main systematic uncertainties that are introduced in the UHECR spectrum measurement with the HiRes detectors have been reported in [6]. They are uncertainties in the absolute phototube calibration ( $\pm 10\%$ ), the fluorescence yield ( $\pm 10\%$ ) and the correction for “missing energy” ( $\pm 5\%$ ). The latter refers to the energy component that is channeled mainly into neutrinos and does not contribute to the ionization process. Not taking into account atmospheric effects, the uncertainty in the energy scale is  $\pm 15\%$ , which results in a systematic uncertainty in the flux  $J$  of  $\pm 27\%$ . The effect on the energy scale of a variation of the average vertical aerosol optical depth (VAOD) by  $\pm 1$  RMS value, from 0.04 to 0.06 and 0.02, has also been described in [6]. It is not larger than 9% on the average. This results in a total uncertainty in the energy scale of  $\pm 17\%$ . The effect of the same VAOD variation on the aperture leads to an average atmospheric uncertainty in the flux  $J$  of  $\pm 15\%$ . The total systematic uncertainty in the measured flux adds up to 31% for each of the two monocular spectrum measurements.

In this paper, we examine additional systematic uncertainties that may affect the calculation of the HiRes aperture in monocular mode. Since the aperture of an air fluorescence detector is a function of the energy of the observed cosmic rays, it has to be modeled carefully with detailed Monte Carlo (MC) simulations. The HiRes MC simulation programs use libraries of air shower profiles, generated at different energies with the air shower simulation program CORSIKA [7] and the hadronic interaction code QGSJet [8], for a realistic representation of the fluctuations in the observed charged particle profiles. A detector response MC program simulates the light emission process along the shower and traces the photons through the atmosphere to the telescopes of the two detectors, taking into account all relevant atmospheric effects. The detector optics, electronics and trigger system are modeled in great detail using databases that record variable detector settings, as well as density fluctuations of aerosols in the atmosphere. After performing extensive comparisons between simulated events and data, which allow us to verify the quality of our simulations (see [9]), we estimate the detector acceptance using the ratio of accepted MC events ( $\nu^{MC}$ ) to generated MC events ( $\mu^{MC}$ ) in each energy

bin. To correctly simulate effects stemming from the finite energy resolution of the detectors and their limited elevation coverage, we use a continuous energy spectrum and a bi-modal composition based on previous measurements as inputs to our simulation programs.

The differential flux  $J$  in each energy bin is calculated as:

$$J(E_i) = N(E_i) \cdot \frac{1}{\Delta E} \cdot \frac{1}{C_i \cdot A\Omega \cdot t} \quad (1)$$

where  $N(E_i)$  is the number of observed events in the energy bin and  $\Delta E$  is the bin-width. The geometrical aperture (area  $\times$  solid angle) used in generating MC events is noted by  $A\Omega$ , and  $t$  is the detector live-time. Through our use of a continuous and realistic input energy spectrum, the finite energy resolution of the detectors is taken into account in the acceptance  $C_i = \frac{\nu_i^{MC}}{\mu_i^{MC}}$ . This will be explained in the next chapter. In the following, we refer to the product of the constant  $A\Omega$  and the acceptance as (instantaneous) aperture.

We will first consider the effects of varying the input energy spectrum on the calculated aperture and thus on the measured spectrum, in Section 2. In Section 3, we examine the implications of exchanging the hadronic interaction model in the air shower generator. For this study, we replace the QGSJet model, which is used in our standard spectrum measurement, with the SIBYLL model [10]. The effect of a variation of the assumed input composition on the measured spectrum is presented in Section 4. Another systematic uncertainty that can affect the aperture estimate of the experiment is that due to variations in the aerosol component of the atmosphere. For the analysis of the monocular spectra, we used an average atmospheric description based on measurements with laser systems that are installed at each detector site [11]. In Section 5, we re-analyze the HiRes-II monocular data with a database containing hourly measurements of the aerosol component of the atmosphere and compare it to the average description in our standard analysis. Although the systematic studies presented in this paper have been carried out with simulation and reconstruction tools of the HiRes-II analysis, their results are applicable to the HiRes-I spectrum measurement as well.

## 2 Input Energy Spectrum Bias

The calculation of the cosmic ray energy spectrum from the measured energy distribution of events is a problem of unfolding the true spectrum of cosmic rays at their arrival at the earth's atmosphere from the distortions introduced by the detector. The energy distribution provided by the detector is a convolution of the true spectrum with the detector response, i.e. the efficiency of

the detector and its finite resolution. Following the discussion in G. Cowan's *Statistical Data Analysis* [12], the problem of unfolding can be stated in the following way:

$$\nu_i = \sum_{j=1}^M R_{ij} \mu_j \quad (2)$$

Here, the true energy spectrum and the measured spectrum are divided into  $M$  energy bins;  $\mu_j$  is the number of events in bin  $j$  of the true histogram,  $\nu_i$  the expectation value of the number of events in bin  $i$  of the measured histogram.  $R_{ij}$  is the response matrix, which describes the detector response in each energy bin. Off-diagonal elements in  $R_{ij}$  are due to the limited resolution of the detector, which distributes a fraction of events from a certain energy bin over adjacent bins.

The most straightforward way of determining the real event distribution  $\mu_j$  from the measured values is to calculate the response matrix and apply its inverse to the measured distribution. Determining the response matrix requires knowledge of the detector resolution and acceptance, as well as a good estimate of the true spectrum. However, as Cowan shows, even with a complete knowledge of  $R_{ij}$ , this method is not applicable in most cases since it leads to large variances in the unfolded histogram, when the resolution is large compared to the bin-width. These variances arise due to the Poisson distribution of the observed data around the expectation values  $\nu_i$ .

In practice, the ‘‘method of correction factors’’ can be applied for the deconvolution of the measured spectrum. This is the method used in our analysis. The estimator  $\hat{\mu}_i$  for the true spectrum is written as:

$$\hat{\mu}_i = C_i^{-1} \cdot n_i \quad (3)$$

where  $n_i$  are the observed data and  $C_i^{-1}$  are multiplicative correction factors for each energy bin. These correction factors are determined with MC simulations of both the physical model under study and the complete measurement process. They are just the inverse of the acceptance estimate  $C_i$ , which is given by the ratio of accepted over generated events in the MC in each energy bin:

$$C_i = \frac{\nu_i^{MC}}{\mu_i^{MC}} = \frac{\nu^{MC}(E_i)}{\mu^{MC}(E'_i)} \quad (4)$$

The distribution of accepted events  $\nu^{MC}$  is evaluated at the reconstructed energies  $E_i$ , whereas the distribution of generated events  $\mu^{MC}$  is given as a function of the true (input) energies  $E'_i$ . Calculation of the expectation value

for the estimator  $\hat{\mu}_i$  provides an expression for the bias of the method of correction factors.

$$E[\hat{\mu}_i] = C_i^{-1} \cdot E[n_i] = C_i^{-1} \cdot \nu_i = \mu_i + \left( C_i^{-1} - \frac{\mu_i}{\nu_i} \right) \nu_i \quad (5)$$

The bias in the estimator  $E[\hat{\mu}_i]$  is given by the last term of Equation 5. It goes to zero as the estimated acceptance,  $C_i$ , approaches the true acceptance of the experiment,  $\frac{\nu_i}{\mu_i}$ . The more realistic the assumptions that go into the MC simulation are, the smaller the bias will be. One can estimate the bias by varying the model used in the simulation.

We have calculated an estimate of the bias by varying the assumed true energy spectrum that is used as an input to the MC. It is useful to rewrite the term that describes the bias in the following way:

$$b_i = \left( C_i^{-1} - \frac{\mu_i}{\nu_i} \right) \nu_i = \left( \frac{\nu_i}{\mu_i} \cdot C_i^{-1} - 1 \right) \mu_i = (R - 1) \mu_i \quad (6)$$

The bias as a fraction of the real spectrum  $\mu_i$  can thus be calculated from the ratio  $R$  of the true to the estimated acceptance. For our bias estimate, we assumed the true acceptance  $\frac{\nu_i}{\mu_i}$  to be the result of a simulation using our best estimate of the input energy spectrum. The estimated acceptance  $C_i$  was calculated using a simple  $E^{-3}$  power law for the input energy spectrum.

Figure 1 shows the measured energy distribution for data and a MC simulation assuming an  $E^{-3}$  input spectrum. About one third of the HiRes-II data used in our monocular spectrum measurement published in [5] have been included in this comparison. As can be seen from the distributions, and more clearly from the ratio plot (lower panel, data divided by MC), this choice of the input spectrum is not very good. The ratio is not flat because the assumed input spectrum does not have a break (“ankle”). Thus, if one normalizes data and MC to the same total number of events, the fraction of MC events is too small at low energies and too large at higher energies. We have used this MC set to calculate the biased acceptance estimate  $C_i$ .

The bias has been corrected in Figure 2: instead of the  $E^{-3}$  spectrum, we now use a fit to the Fly’s Eye stereo spectrum [13] to determine the shape of the input spectrum below the “ankle”, and a linear fit to the HiRes-I spectrum for higher energies. The spectral index of this input spectrum is -3.01 between  $10^{16.5}$  eV and  $10^{17.6}$  eV, -3.27 between  $10^{17.6}$  eV and  $10^{18.7}$  eV, and -2.80 above  $10^{18.7}$  eV. In this study, the position of the “ankle” is assumed to be at  $10^{18.7}$  eV, corresponding to the first results of the HiRes spectrum measurements published in [9]. Our more recent result with higher statistics in the HiRes-II

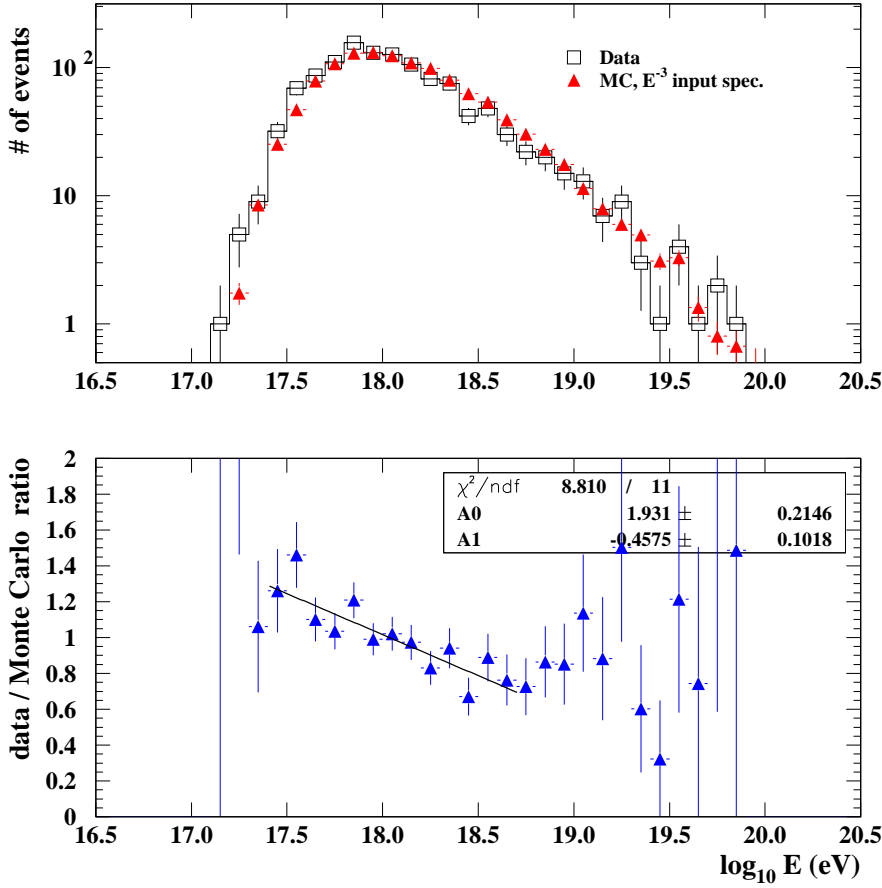


Fig. 1. The top panel shows the energy distribution of HiRes-II data. The histogram and square points show the actual data; the triangles show the MC distribution, *assuming an  $E^{-3}$  input spectrum*, normalized to the same total number of events. The bottom panel shows the ratio of the data to MC distributions from the top plot with a linear fit below the “ankle”.

data-set observes the “ankle” at  $10^{18.5}$  eV. The linear fit above the “ankle” is extended to the highest energies. The good agreement between data and MC shows that this choice of input spectrum is closer to the true spectrum  $\mu_i$  given that the MC simulates all other aspects of the experiment well, which was shown in [9]. This MC set is used to estimate the true acceptance  $\frac{\nu_i}{\mu_i}$ .

The nearly flat ratio of the data and MC distributions in Figure 2 means that  $\frac{\nu_i}{\nu_i^{MC}}$  is approximately constant if one chooses a realistic input spectrum. In this case, according to Equation 5, the energy dependence of the expectation value for the true spectrum  $E[\hat{\mu}_i]$  is approximately given by the input spectrum  $\mu_i^{MC}$ . Any differences in the unfolded spectrum can be fed back into the MC and will improve the agreement between the energy distributions in real and simulated data, thus reducing the bias in the spectrum calculation with the updated MC simulation.

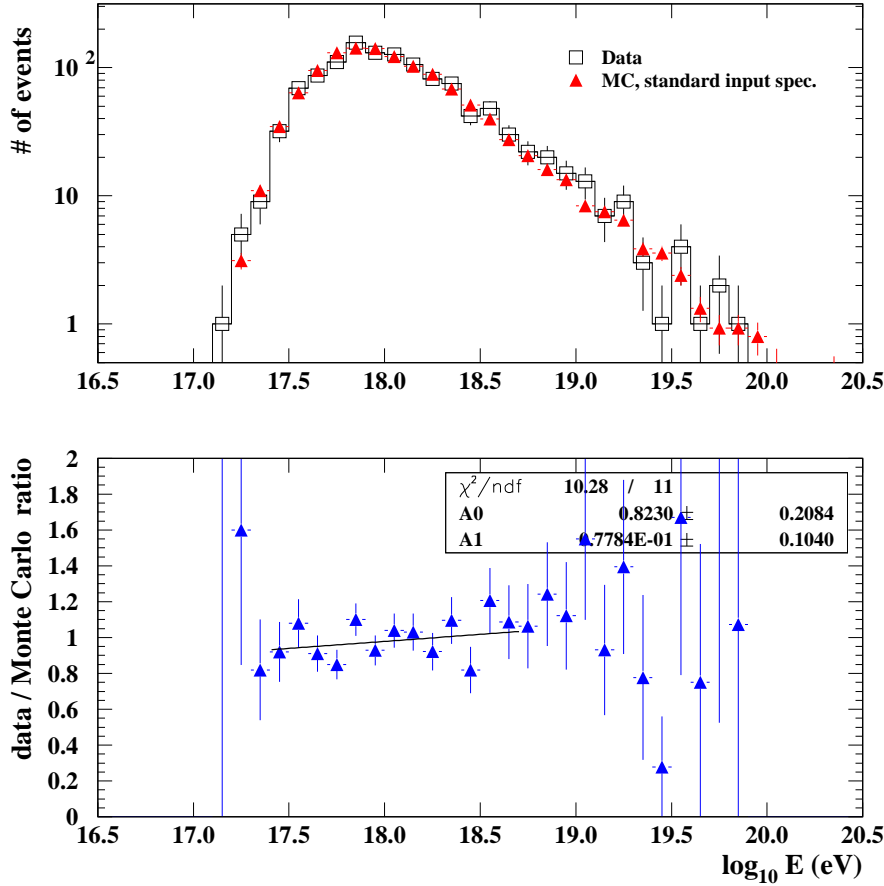


Fig. 2. The top panel shows the energy distribution of HiRes-II data. The histogram and square points show the actual data; the triangles show the MC distribution, *assuming an input spectrum based on broken power law fits to the Fly’s Eye stereo spectrum [13] and HiRes-I spectrum [6], normalized to the same total number of events.* The bottom panel shows the ratio of the data to MC distributions from the top plot with a linear fit below the “ankle”.

The bias we avoid by including the “ankle” feature in the input spectrum can be derived from Figure 3 which shows the ratio  $R$  of acceptances for the two MC simulations. A kink is visible in the ratio plot in the “ankle” region, even though the effect is very small. The ratio increases from  $\sim 0.97$  at  $10^{18}$  eV to  $\sim 1.07$  at  $10^{18.5}$  eV and then decreases to  $\sim 0.94$  at  $10^{18.8}$  eV. This bias is due to the limited energy resolution of the detectors which spreads event energies over neighboring bins. It should be noted that the same random number seeds have been used in both MC sets to reduce statistical fluctuations in the ratio plot. In our standard analysis, we smooth the calculated acceptance by replacing the acceptance histogram with an appropriate fitting function. The remaining statistical fluctuations are then taken into account in the spectrum measurement. For this study, we have not applied any smoothing procedures.



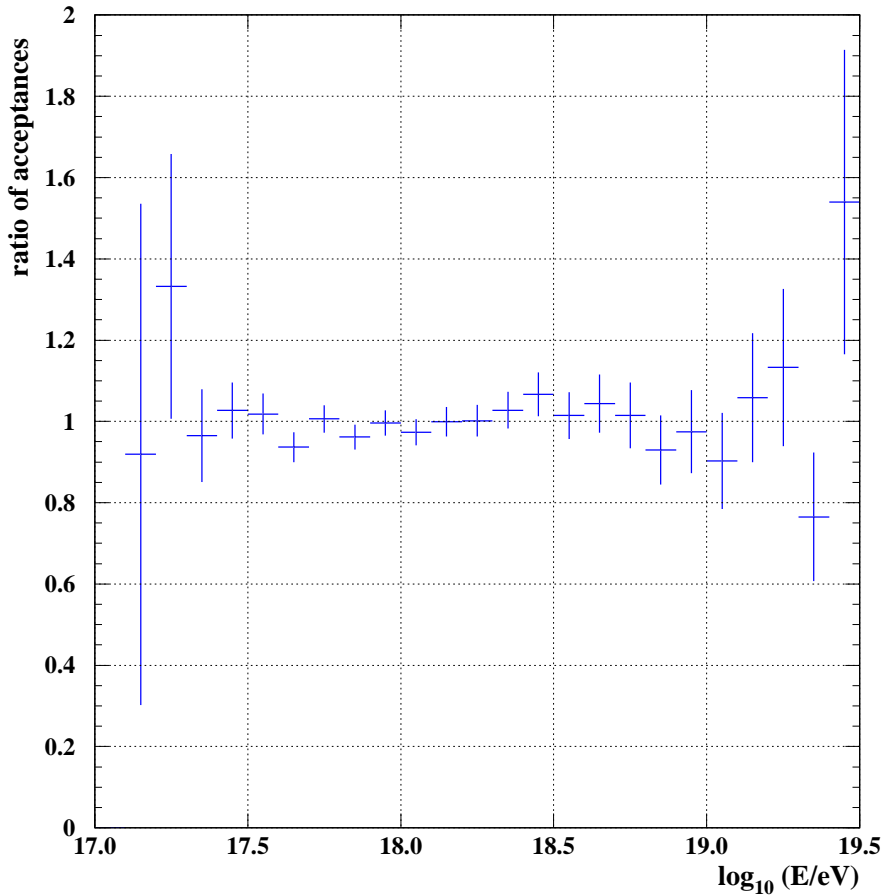


Fig. 3. Ratio of the acceptance calculated using an input spectrum based on the Fly’s Eye and HiRes-I measurements, as described in the text, to the acceptance calculated assuming an  $E^{-3}$  input spectrum.

In our analysis of the HiRes-II spectrum, we used initially an  $E^{-3}$  input spectrum, which was soon replaced by a spectrum with the shape of the Fly’s Eye measurement [13]. This input spectrum was used for our publication of the monocular spectra [6], [9]. Our measurement of the position of the “ankle” and the spectral index above the “ankle”, as described above, was used for our updated spectrum publication [5]. Adjusting the input spectrum to feature the “ankle” shape has helped us to significantly improve the agreement in several comparison plots between data and MC events, which we use to evaluate our simulation programs. The effect on the acceptance is rather small, as seen in Figure 3. Replacing the  $E^{-3}$  input spectrum with an “ankle” shape led to a variation in the acceptance of less than 10%. Any further adjustments of the exact shape of the “ankle” had negligible effects on the spectrum.

Thus far, we have not included the observed flux suppression [5] above  $10^{19.8}$  eV in our input energy spectrum.

### 3 Hadronic Interaction Model Uncertainty

When simulating events, we read profiles of charged particles from a library of air showers and simulate the light generation, propagation, and detector response for different shower geometries. This “shower library” contains a large collection of profiles in steps of 5 g/cm<sup>2</sup> vertical atmospheric depth at several fixed energies and at a zenith angle of 45°. The shower profiles were generated with CORSIKA for proton and iron primaries and fitted with the Gaisser-Hillas function [14]:

$$N(X) = N_{max} \left( \frac{X - X_0}{X_{max} - X_0} \right)^{(X_{max} - X_0)/\lambda} \exp(-(X_{max} - X)/\lambda) \quad (7)$$

The three fit parameters,  $X_{max}$  (the atmospheric slant depth at shower maximum),  $N_{max}$  (the number of charged particles at shower maximum) and  $\lambda$ , were written into the library files for each shower to characterize its profile.  $X_0$  was fixed at -60 g/cm<sup>2</sup>. Correlations between the mean values of the fit parameters and the logarithm of the shower energy are used to scale shower profiles from the fixed energies provided in the library to the continuous energy spectrum required in the detector response MC, as described in [9]. Our analysis uses Gaisser-Hillas fits to the charged particle profiles of air showers to estimate the ionization energy of observed and simulated showers. The integral over the fitted profile is multiplied by a mean ionization loss rate, derived from simulations with CORSIKA to be 2.19 MeV/(g cm<sup>2</sup>) [15]. Before the integration is carried out on MC events, the particle profile has to be adjusted for a fraction of 10% of the primary energy that is lost due to cuts on particles with energies below preset thresholds in CORSIKA. We then also have to determine the “missing energy”, which does not contribute to the ionization process, by comparing the estimated ionization energy of the library showers to their known total energy. A correction for the “missing energy” is added to the reconstructed energies of all simulated and real events.

Newer CORSIKA versions provide directly information on the energy deposit profile of the air shower, but in this study we want to apply the same algorithms used in our published analysis of the monocular spectra. We have verified that our method yields results consistent with the energy deposit profiles.

The physics contributing to the electromagnetic component of the air shower is well understood and described in detail by the EGS code [16] within the CORSIKA program framework. The main uncertainty in the air shower simulation stems from our limited knowledge of the initial hadronic interactions, which take place at energies by far exceeding those that can be observed in the laboratory. In order to get an estimate of the influence of those uncertainties

on the calculated aperture, we have generated two “shower libraries” using two different hadronic interaction models. CORSIKA 5.61 with QGSJet01 [8] has been used in our standard analysis. For this study, we generated an updated shower library with CORSIKA 6.022 and QGSJet01. The second model we chose was SIBYLL 2.1 [10] (with the same CORSIKA version). Differences between the two models can be found in their predictions of the particle multiplicity, inelasticity and the extrapolations of the hadron-air cross-section to ultra-high energies. A detailed comparison is given in [17]. With regard to the charged particle profiles we are interested in, differences can be seen in the mean  $X_{max}$  values and the elongation rates ( $\frac{d\langle X_{max} \rangle}{d\log(E)}$ ). SIBYLL showers, especially in the case of proton primaries, have on average larger  $X_{max}$  values and a slightly different elongation rate, as can be seen in Figure 8 (in the next chapter). Another difference between the two models is shown in Figure 4. Our estimates of the ionization energy fraction are roughly 2% larger when using SIBYLL, as compared with QGSJet.

For the estimation of the detector aperture, we follow the same procedure with each of the two hadronic interaction models: the fit parameters for the “shower libraries” are taken from Gaisser-Hillas fits to the shower profiles. We found that the Gaisser-Hillas function with three parameters describes accurately the particle profiles for showers generated with either of the two hadronic interaction models. We determine the MC input composition from HiRes/MIA and HiRes stereo measurements of the mean  $X_{max}$  as a function of the cosmic ray energy. At a given energy, the mean  $X_{max}$  of the air shower distribution is correlated with the average mass of the primary cosmic ray flux. We assume a simple bi-modal composition of protons and iron nuclei and determine a proton fraction by comparing the data points with the iron and proton estimates given by the two models. This procedure will be described in more detail in the following chapter.

Since the mean  $X_{max}$  values for pure proton showers are larger in the case of SIBYLL, we had to re-calculate the proton fraction that corresponds to the data points and adjust the input composition to contain a larger fraction of iron showers. The difference in the proton fractions used as input to the MC for the two models are shown in Figure 5. The  $X_{max}$  distributions of reconstructed MC events that passed all our quality requirements are shown in Figure 6 for the two models. The close agreement of the distributions for the QGSJet and SIBYLL simulations demonstrates that we place simulated showers at the same distribution of atmospheric depths for either model.

In both cases, we determine the “missing energy” from a comparison of the total shower energy to the integral of the shower profile that has been multiplied by the mean ionization loss rate. Instead of applying an average correction for proton and iron showers, we determine the correction for the fraction of simulated proton and iron showers that were accepted in our detector response

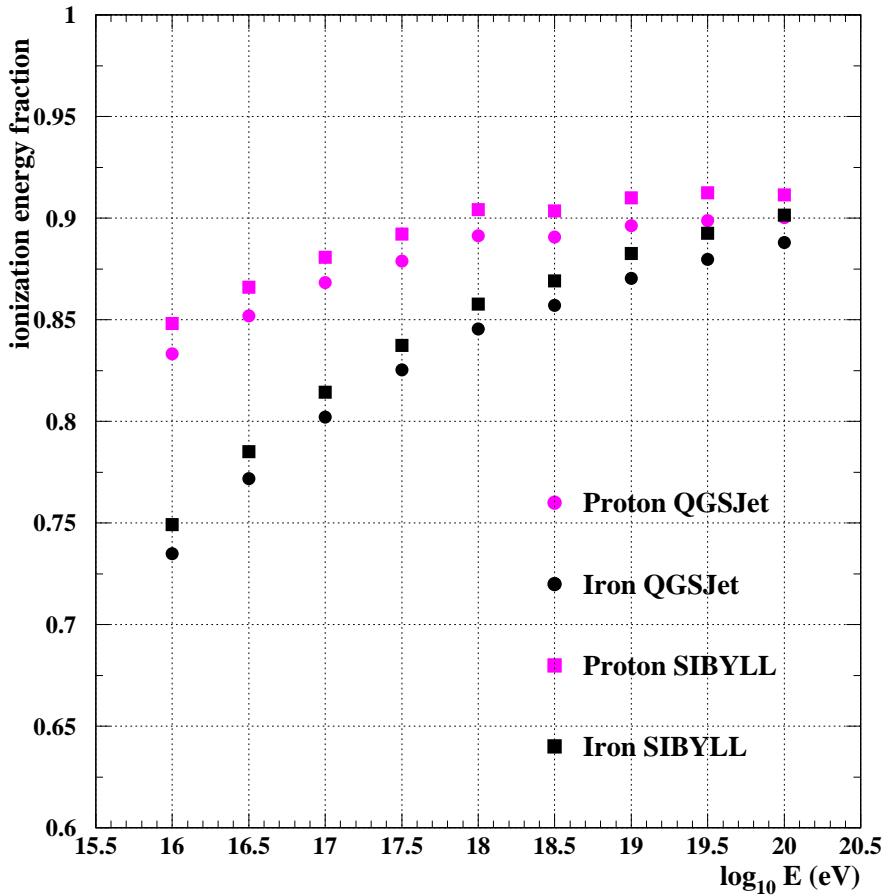


Fig. 4. Estimates of ionization energy fraction derived from shower profiles. The ratio of ionization energy to total energy is shown for proton (upper points, in magenta) and iron primaries (lower points, in black) versus the logarithm of the total energy. The squares are results from simulations with SIBYLL, the circles correspond to QGSJet.

simulation and successfully reconstructed.

Using the same analysis procedure for each of the two hadronic interaction models, we did not find any significant differences in our extensive set of comparisons between distributions of data and simulated events with the two MC sets. Figure 7 shows the ratio of the apertures that result from simulations using the QGSJet and SIBYLL libraries of air showers. No smoothing algorithms have been applied to the calculated acceptances. The same random number seeds were used for the two MC sets to reduce statistical fluctuations. Both the normalization, which is consistent with 1, and the zero slope of the fit to this ratio show that the effect is negligible compared to the statistical uncertainties in our data-set. We thus find that if we apply our procedure to estimate the detector aperture in a consistent way, the result does not depend on the chosen hadronic interaction model. This is important since the

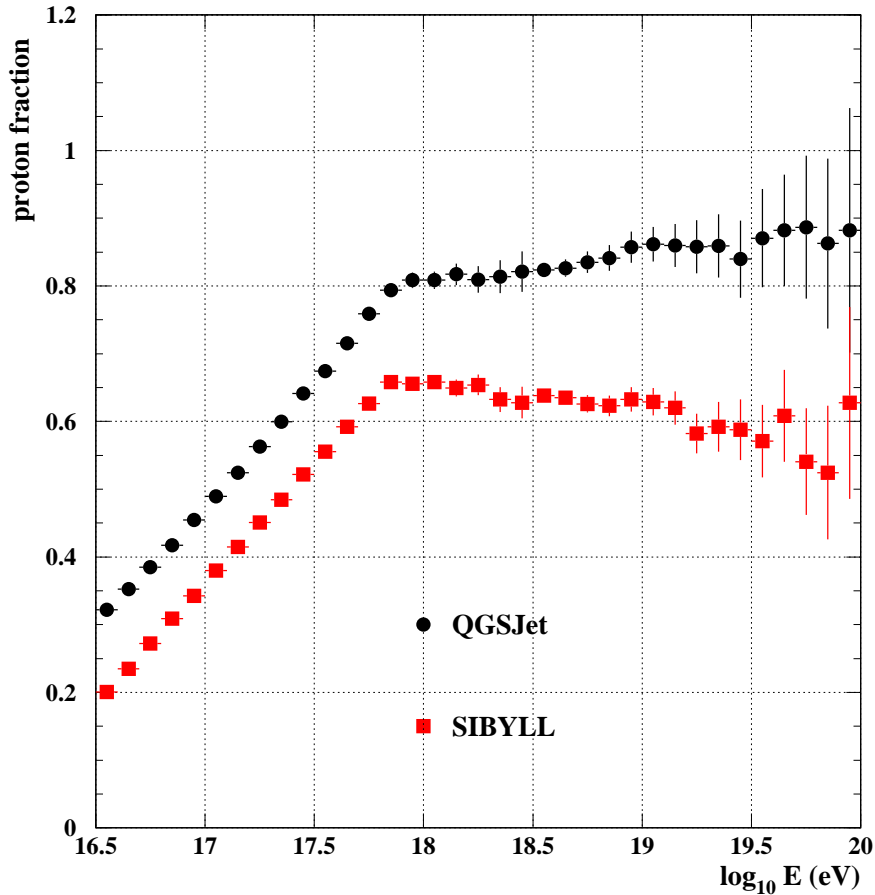


Fig. 5. Proton fractions used for the MC input composition for QGSJet and SIBYLL.

models are continuously evolving. The latest version of the QGSJet model (QGSJet02) for example has been shown to generate mean  $X_{max}$  values closer to the predictions of SIBYLL 2.1 [18].

#### 4 Input Composition Uncertainty

The fraction of air showers initiated by light and heavy (i.e. proton and iron) cosmic rays used in our MC simulation is determined from composition measurements by the HiRes/MIA [19] [20] and HiRes Stereo [21] experiments. Air fluorescence detectors like HiRes can measure the cosmic ray composition as a function of energy in a statistical way. The atmospheric depth,  $X_{max}$ , at which an extensive air shower reaches its maximum size depends not only on the energy but also on the mass of the primary cosmic ray particle. On the average, heavy nuclei interact higher in the atmosphere than light nuclei of the same energy. Nuclei break up into fragments, each of which generates a

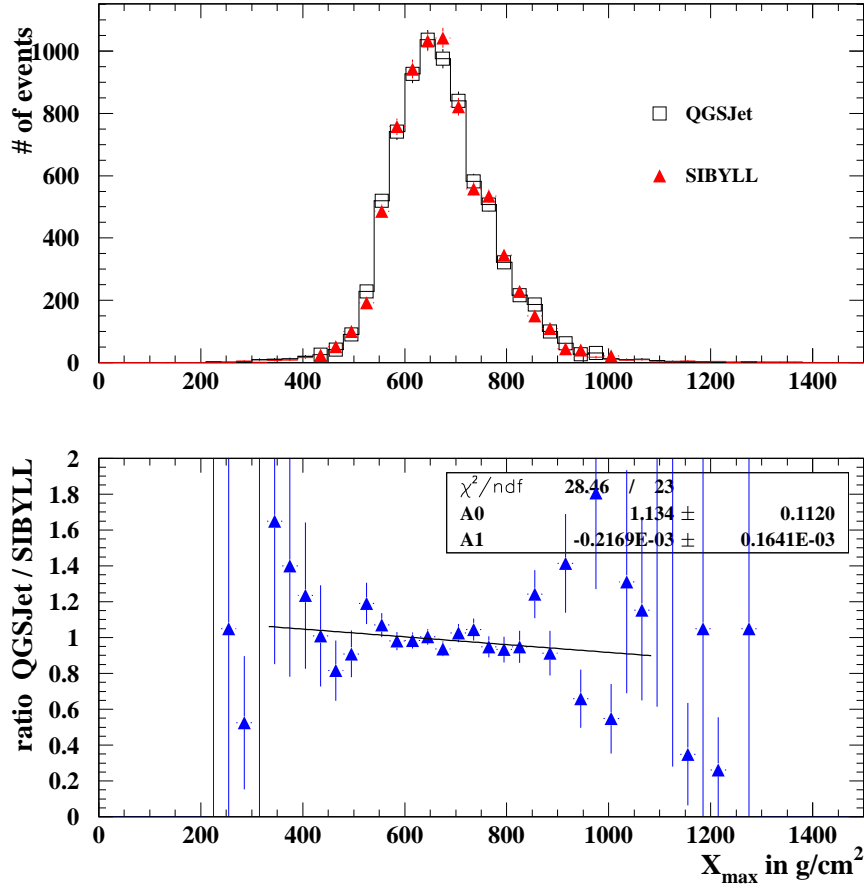


Fig. 6. The top panel shows the MC distributions of reconstructed  $X_{max}$  using QGSJet (squares) and SIBYLL (triangles). The two distributions have been normalized to cover the same area. The bottom panel shows the ratio of the two distributions shown in the top panel.

sub-shower, thus distributing the initial energy over several cascades. (In a highly simplified picture, an iron shower is approximated by the superposition of 56 proton showers of a factor of  $1/56$  smaller energies.) Unfortunately, statistical fluctuations between shower profiles are large and do not allow an event-by-event determination of the cosmic ray composition. Only the  $X_{max}$  distribution for a given energy bin can be measured and compared to model predictions of protons and iron nuclei.

Figure 8 shows the measured mean  $X_{max}$  together with the pure proton and iron estimates from different models. We have re-interpreted the HiRes/MIA measurement by comparing it against the QGSJet01 model [8]. We use linear fits to the HiRes/MIA and HiRes Stereo points to determine an energy dependent proton fraction  $f(E)$  by comparing the fits with the simulated iron and proton lines of QGSJet01. In this simple bi-modal model, we derive  $f(E)$  from the distance of the fitted data points to the proton and iron lines. A data

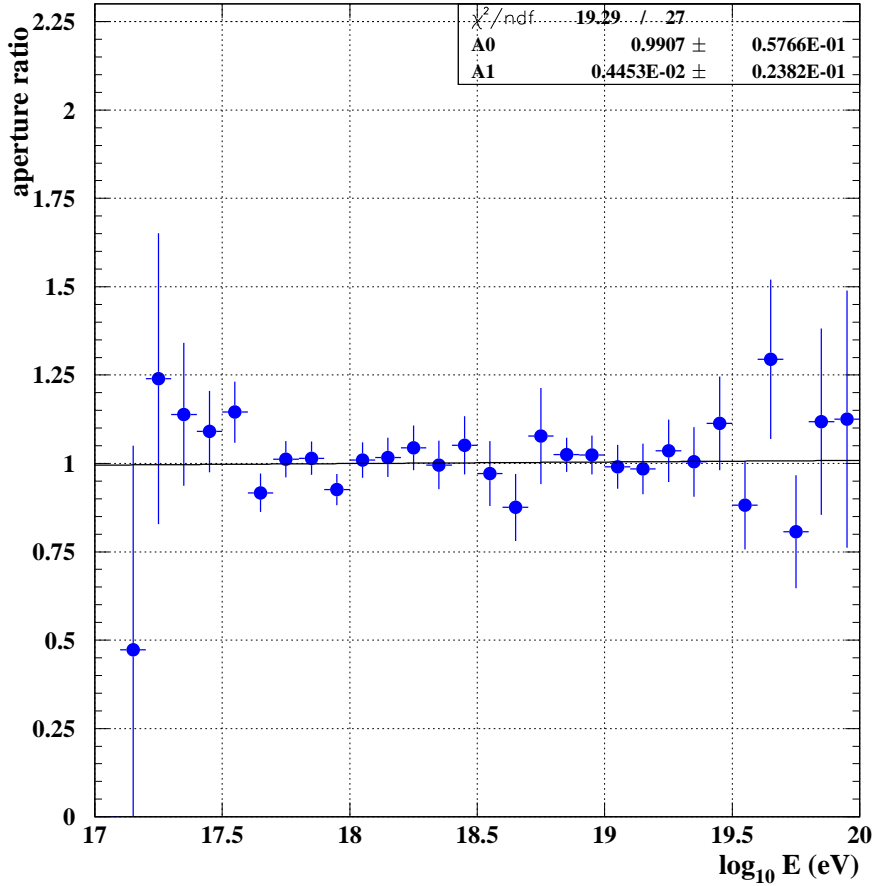


Fig. 7. Ratio of apertures using SIBYLL 2.1 (numerator) and QGSJet01 (denominator) with linear fit.

point on the proton line would have an  $f$  of 1, whereas a data point in the middle between the two simulation lines would have an  $f$  of 0.5. The derived proton fraction is 0.45 at  $10^{17}$  eV, 0.80 at  $10^{17.85}$  eV and 1.0 at  $10^{20}$  eV. The proton fraction we determine from the measurements and insert into our MC simulations depends thus on a specific interaction model. However, by using the same model as a reference for the input composition and for the simulation of air showers, we generate events with the measured  $X_{max}$  distribution independently of the chosen model, as was shown in the previous section.

Here, we investigate the effect of a change in the measured mean  $X_{max}$  on our aperture estimate. For this study, we have used the same MC programs as in our standard analysis, i.e. the HiRes-II detector response simulation and CORSIKA 5.61 with QGSJet01 for the air shower generation. The difference in the estimated aperture between a MC set with only iron events and a set with only proton events can be seen in Figure 9. At the low energy end of the spectrum, the aperture for iron cosmic rays is lower because iron showers develop higher up in the atmosphere and are more likely to lie above the

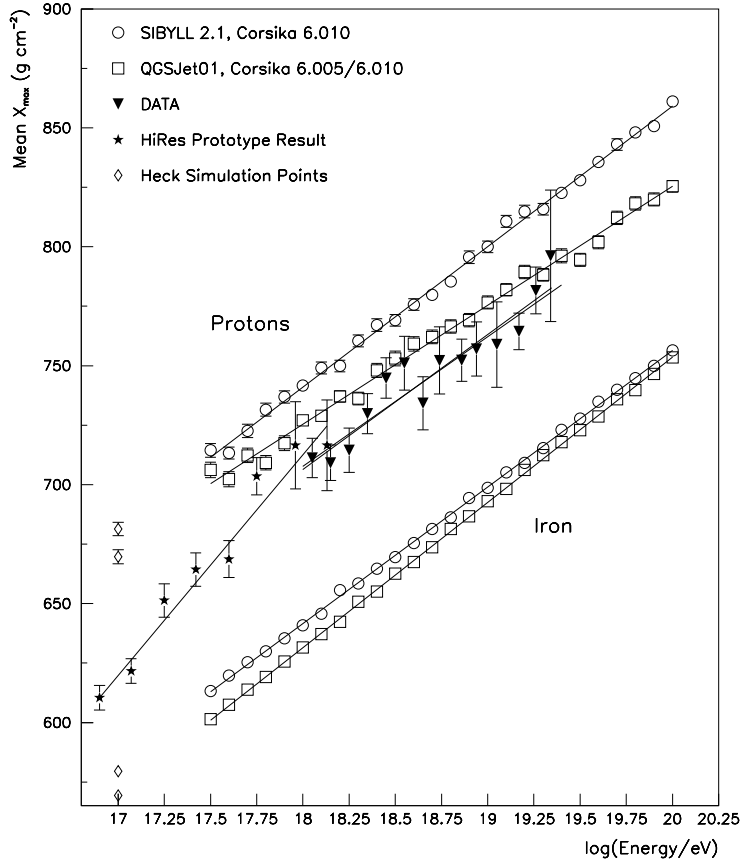


Fig. 8.  $X_{max}$  vs. the logarithm of the energy from HiRes/MIA (stars) and HiRes Stereo (triangles) measurements. The predictions for QGSJet and SIBYLL are shown for comparison. The diamonds are simulation points calculated by D. Heck. The best fit to each data set is shown. A fit to the 76% of HiRes Stereo data with hourly atmospheric corrections is included as well. This fit has a slightly steeper slope. The figure is taken from [21].

HiRes-II elevation coverage ( $3^\circ$  to  $31^\circ$ ) than proton showers. This leads to larger differences between the two apertures at lower energies. For energies above  $\sim 10^{18}$  eV, where showers are on average farther away from the detector, no significant difference is seen in the aperture for iron and proton showers.

Using the pure iron and pure proton apertures, we have calculated the effect of a change in the assumed proton fraction on the aperture estimate. The proton fraction  $f(E)$  is defined as the ratio of generated proton showers over the sum of generated proton and iron showers in the MC:  $f(E) = \mu_p(E)/(\mu_p(E) + \mu_{fe}(E))$ . The acceptance for a MC set with a proton fraction  $f$  in a given



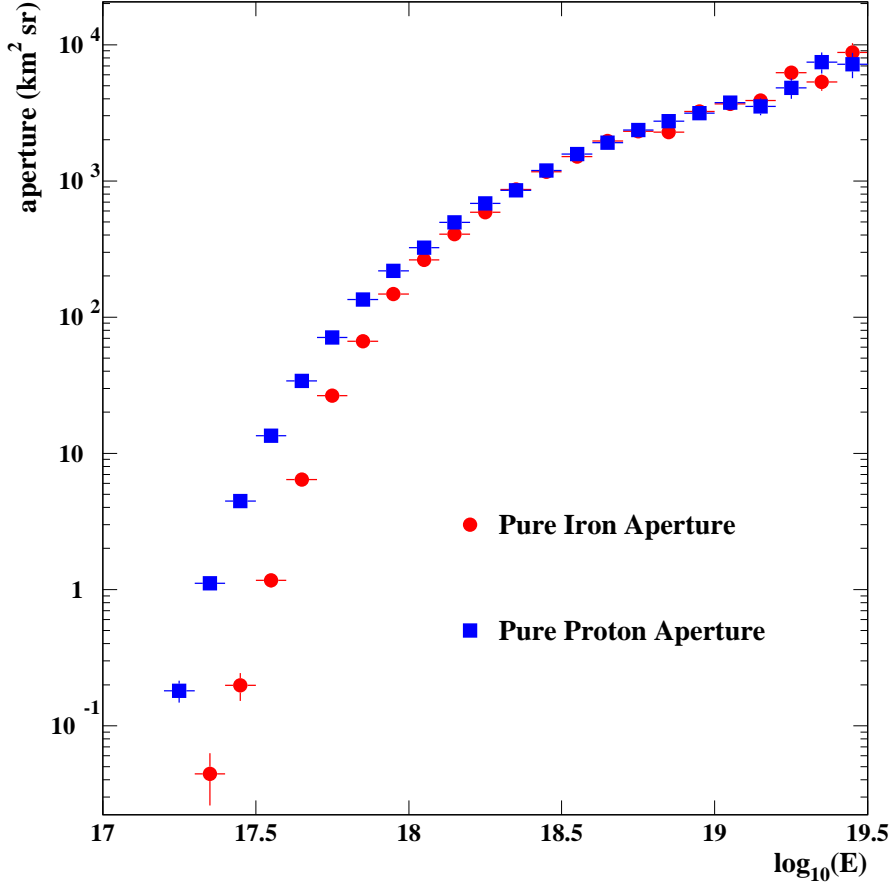


Fig. 9. Apertures for pure iron and pure proton MC sets.

energy bin is:

$$a_f = \frac{\nu_p + \nu_{fe}}{\mu_p + \mu_{fe}} = \frac{\nu_p(1 + \nu_{fe}/\nu_p)}{\mu_p/f} = a_p(R + f \cdot (1 - R)) \quad (8)$$

Here  $\nu_p$  and  $\nu_{fe}$  are the accepted, i.e. triggered and well reconstructed, proton and iron events, respectively;  $a_f$  and  $a_p$  are the acceptances for a MC set with proton fraction  $f$  and 1, respectively.  $R$  is given by the ratio of the acceptances for pure iron and pure proton MC sets  $\left(\frac{\nu_{fe}/\mu_{fe}}{\nu_p/\mu_p}\right)$ . This ratio can be determined directly from the two curves shown in Figure 9, since the apertures are just the acceptances multiplied by a constant factor, the geometrical aperture  $A\Omega$ . With  $R$  known, Equation 8 yields the acceptance  $a_f$  for a given proton fraction  $f$  in a given energy bin.

It can be seen from Figures 9 and 8 that systematic uncertainties in the aperture due to uncertainties in the proton fraction are only of concern at the low energies covered by the HiRes/MIA measurement. We have calculated the sys-

tematic uncertainty in the proton fraction  $f(E)$  from the relevant uncertainties in energy and  $X_{max}$  quoted in the HiRes/MIA PRL paper [20].

Sources for energy uncertainties in HiRes/MIA are the detector calibration (<5% uncertainty in energy) and the aerosol component of the atmosphere (<10% uncertainty in energy). A 10% uncertainty in the fluorescence yield is common to both HiRes and HiRes/MIA, and is therefore not included in our calculation. Since both experiments use the same assumptions on the fluorescence yield, a potential error in this parameter would induce the same bias in the reconstructed energies of HiRes/MIA and HiRes. It would thus not change the shape of the aperture. Given the measured elongation rate of 93 g/cm<sup>2</sup> [20], the uncertainties in energy from calibration and atmosphere, added in quadrature, contribute <4.4 g/cm<sup>2</sup> to the uncertainty in  $X_{max}$ .

The quoted uncertainty in  $X_{max}$  of roughly 25 g/cm<sup>2</sup> due to the calculation of the Cherenkov fraction is also common to the two experiments and is thus not relevant for our calculation. Since the same assumptions on the Cherenkov light beam are made in the HiRes and HiRes/MIA analysis, a potential bias in the HiRes/MIA reconstruction would be corrected in the HiRes detector simulation before the calculation of the acceptance. In other words, the HiRes MC simulation positions showers on the average at the same height where they were seen by HiRes/MIA. A recent study of the fluctuations of the molecular density profile using radio sonde data shows a small discrepancy with the standard model used in both HiRes/MIA and HiRes [22]. This introduces an additional uncertainty in  $X_{max}$  of <10 g/cm<sup>2</sup>.

Since the separation between the proton and iron lines in the QGSJet01 model is  $\sim 100$  g/cm<sup>2</sup>, the uncertainties in  $X_{max}$  of 4.4 g/cm<sup>2</sup> from the energy measurement and of 10 g/cm<sup>2</sup> from the molecular density fluctuations translate to  $\sim 4.4$  % and  $\sim 10$  % uncertainty in the proton fraction  $f(E)$ , respectively. Finally, one has to add a  $\sim 3$ % uncertainty coming from the linear fit to the HiRes/MIA data that is used to parameterize the proton fraction in the simulation programs. Those uncertainties in the HiRes/MIA measurement of the mean  $X_{max}$  that translate into uncertainties in the acceptance add then up to  $\sim 11$ % of the proton fraction.

With the help of equation 8, we have calculated the variation in the aperture  $a_f(E)$  for a variation in  $f(E)$  of  $\pm 11$ %. A change in the aperture translates directly into a change of the measured spectrum. The uncertainties in the spectrum from a  $\pm 11$ % variation in the proton fraction are shown in Figure 10 as thick error bars. At the low energy end of the HiRes-II spectrum, the systematic uncertainties from the input composition are comparable to the statistical uncertainties in the spectrum. In the absence of a more precise composition measurement in the HiRes/MIA energy range, it will thus be difficult to observe the feature of the “second knee” [23],[24],[25],[26], even

with better statistics in the HiRes-II data. Above  $\sim 10^{18}$  eV, the effect on the aperture estimate becomes negligible.

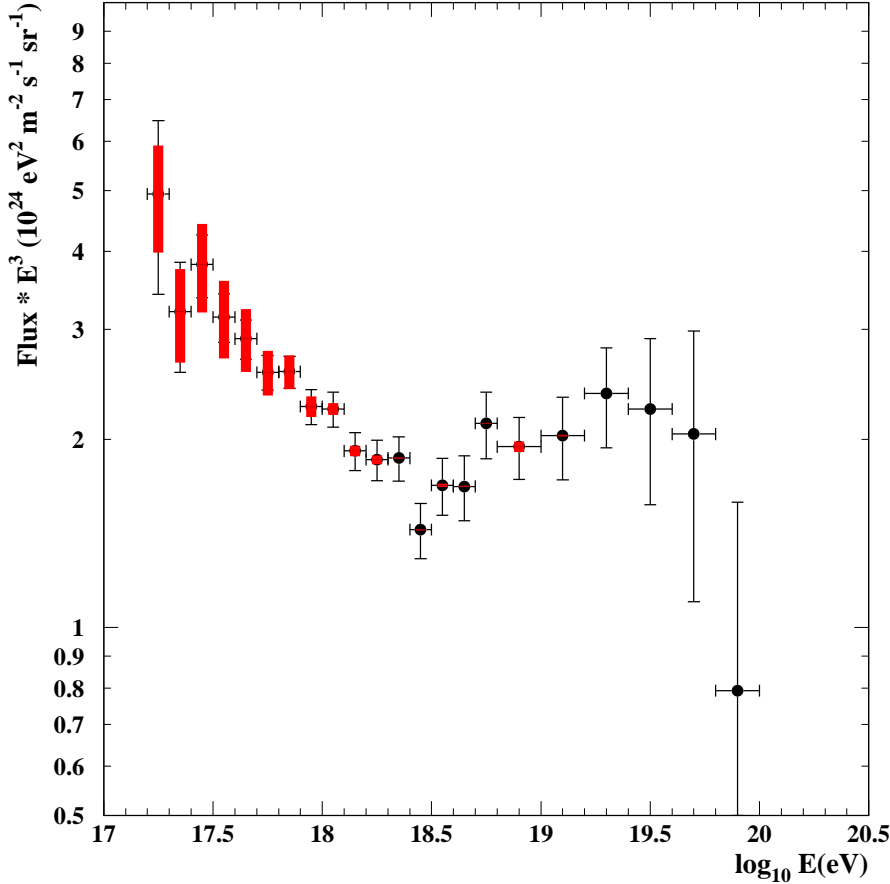


Fig. 10. HiRes-II energy spectrum with systematic uncertainties (thick error bars) corresponding to a  $\pm 11\%$  change in the proton fraction of the MC. Data included in the spectrum were recorded between December 1999 and September 2001.

## 5 Atmospheric Uncertainties

In the ultraviolet (UV) fluorescence range observed by the HiRes telescopes (310-400 nm), light attenuation comes from mainly two sources: Rayleigh scattering on air molecules, and absorption and scattering on aerosols. While Rayleigh scattering is well understood and does not vary much over time, attenuation by aerosols can change over short time ranges and has to be monitored during the data taking process. We use a system of steerable lasers, one at each of the two detector sites, to measure light attenuation by aerosols on an hourly basis. The UV laser at each site fires shots in a regular pattern of varying geometries, which are observed from the other site. The vertical aerosol

optical depth (VAOD) can be measured from the detected light of vertical shots. Horizontal attenuation length (HAL) and scattering phase function due to aerosols can be measured from the light scattered into the telescopes under different angles from horizontal shots. The wavelength of the laser is 355 nm, close to the 357 nm fluorescence line. We account for the wavelength dependence of aerosol scattering in our simulation and reconstruction programs.

For the monocular spectra published in [5] and [6], we used a measurement of the average VAOD and HAL in our analysis. This was necessary since the steerable laser system became fully operational only two years after the HiRes-I detector had started taking data. For consistency in the analysis of the two monocular spectra, we have thus used a single average measurement, while applying strict cuts on the selection of clear nights that were included in the spectrum. Here, we repeat the analysis for HiRes-II using a database with hourly entries of the measured VAOD and HAL instead of the average values.

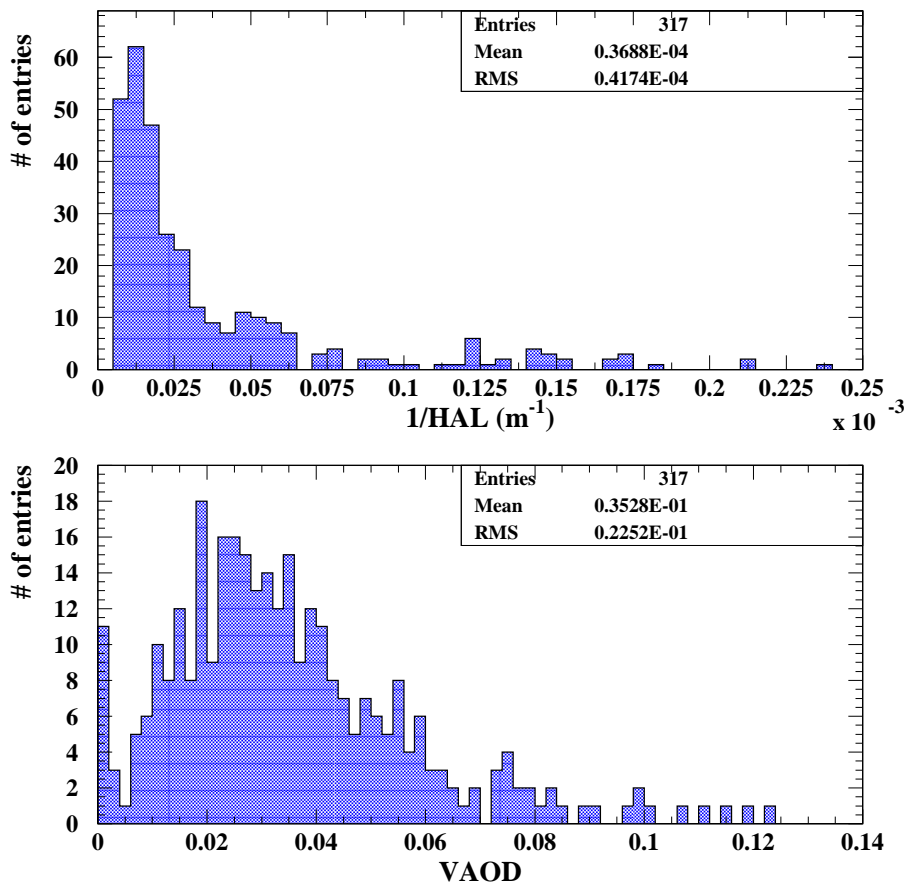


Fig. 11. Hourly VAOD and inverse HAL measurements for the selection of clear nights in the HiRes-II analysis (December 1999 to September 2001).

The inverse HAL and VAOD distributions for the selected clear nights that

went into this analysis are shown in Figure 11. In the atmospheric database generated for the HiRes-II analysis, entries are available for 82 out of the 122 nights that were selected for the spectrum calculation. When measurements of both parameters were not available, a seasonal average was assumed. The averages found in this analysis represent a slightly clearer atmosphere than the values used in the standard monocular analyses ( $\langle \text{HAL} \rangle = 25$  km and  $\langle \text{VAOD} \rangle = 0.04$  were used for our published spectra). This difference is due to the data normalization method applied here, which was not used in the original analysis (see [11] and [27]). The averages determined here ( $\langle \text{HAL} \rangle = 27$  km and  $\langle \text{VAOD} \rangle = 0.035$ ) are nevertheless well within the quoted uncertainties of the averages used in the monocular analyses.

In order to study the effect of variations in the aerosol component of the atmosphere on the reconstructed energies, we have analyzed the HiRes-II data from December 1999 to September 2001 using the atmospheric database. Since all events were reconstructed both with the atmospheric database and with the average atmospheric values, the ratio of the energy estimates can be calculated for each event. The distribution of those ratios is shown in Figure 12 as a function of the energy reconstructed using the atmospheric database. A Gaussian fit has been applied to the distribution in each energy bin. The points represent the Gaussian means, the error bars the standard deviations. The energies reconstructed with database are on the average 4% smaller. This is due to the slightly clearer atmosphere determined with the improved analysis method for the VAOD values that went into the database. There is no significant energy dependence in the ratio of the energies.

We then examined the effect of the small shift in reconstructed energies on the distribution of events over energy bins  $N(E_i)$ , which goes into the spectrum calculation. The histograms for the two energy reconstructions, using the average atmosphere and the atmospheric database, can be seen in Figure 13. The 4% shift in energy is too small to cause a significant effect in the event distribution given our bin-size, which is adapted to the data statistics. It should be noted that the difference between the two distributions is here even aggravated by the fact that two slightly different versions of our reconstruction software were used. The histogram for the average atmosphere is the exactly same as in the calculation of the published HiRes-II spectrum, which permits a direct comparison of this figure with Figure 15, whereas for the reconstruction with database we had to use a slightly updated version of our analysis software. (For Figure 12, only the updated version was used.)

The effect of atmospheric variations on the energy resolution can be studied with simulated events. We have generated a MC set with about four times data statistics using the atmospheric database. The MC events have been reconstructed in two different ways: first with the seasonally averaged atmospheric values and then with the database for nights when atmospheric data

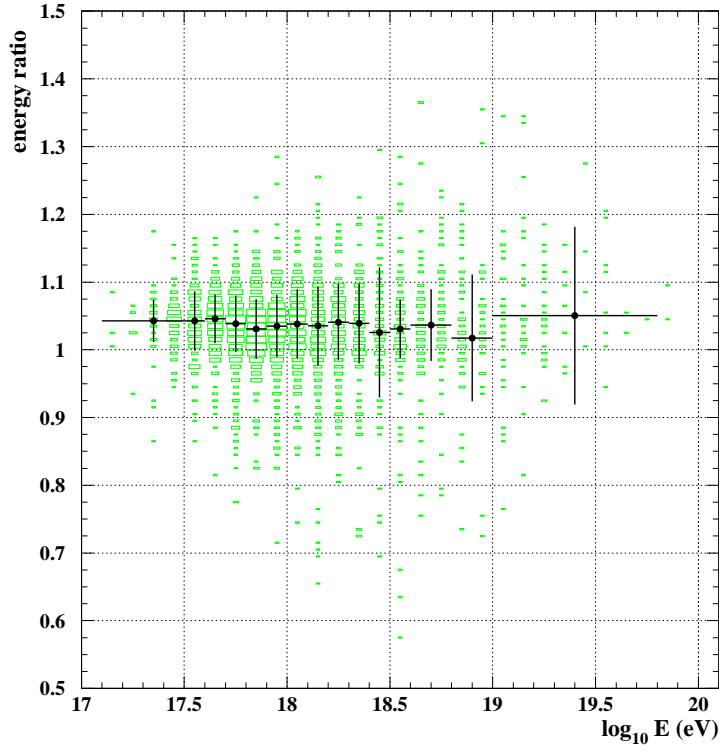


Fig. 12. Difference in reconstructed energies due to atmospheric variations. The energy of each data event has been reconstructed using both the atmospheric database and an average atmosphere. Shown is the ratio of the two reconstructed energies (average over database) versus the energy reconstructed using the atmospheric database. The sizes of the boxes are proportional to the number of entries. The markers represent the mean and width of a Gaussian fit to the distribution in each energy bin.

were available. A comparison of the resolution estimates is shown in Figure 14. It should be noted that the two plots use a logarithmic scale, hence the tails in the distributions are very small. There is no significant difference between the tails of the two distributions. Only the width differs by a small amount. Reconstructing the MC events with seasonally averaged atmospheric values instead of using the atmospheric database widens the resolution by 0.9% (both in RMS and  $\sigma$  of the Gaussian fit).

Finally, we have analyzed the effect of using the atmospheric database rather than the measured average on the energy spectrum. We have calculated the acceptance from a MC set that was generated and reconstructed with the database. As in our standard analysis, we have applied a smoothing procedure to minimize statistical fluctuations in the acceptance. The remaining statistical uncertainties of the smoothed acceptance are taken into account in the measurement of the spectrum. The HiRes-II data were also reconstructed with use of the atmospheric database. In this way, the hourly measurements of

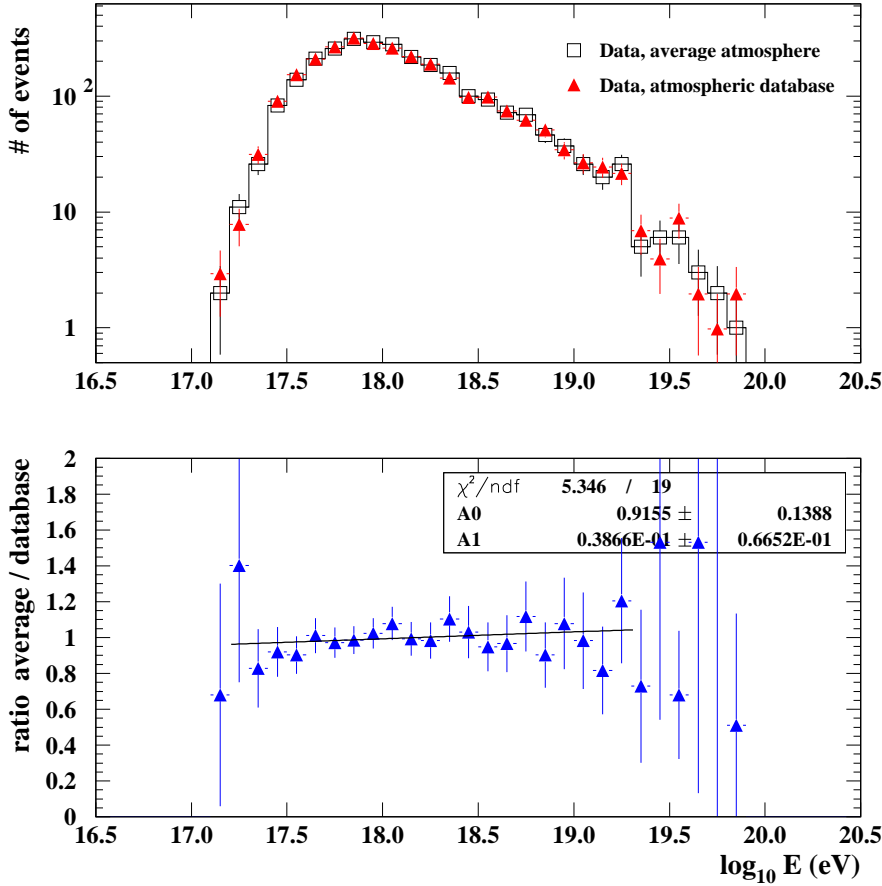


Fig. 13. The top panel shows the energy distribution of HiRes-II data analyzed using the atmospheric database (triangles) and analyzed using average atmospheric parameters (squares). The bottom panel shows the ratio of the two distributions with the average atmosphere case as the numerator and the atmospheric database case as the denominator.

atmospheric variations were included in every step of the analysis. The energy spectrum resulting from this analysis is compared to the published spectrum, which uses the nominal averages of VAOD (0.04) and HAL (25 km), in Figure 15. The result for  $JE^3$  does not vary by more than  $\pm 15\%$  at any energy, except for the first and the last two bins, where statistics in the data are limited. The difference between the two spectra in the last two bins is due to a single event that has shifted up in energy to the last bin when reconstructed using the atmospheric database, as can be seen from Figure 13.

The focus of the study presented in this chapter was on the difference between reconstruction results with an atmospheric database and with an average atmosphere. We have also examined the systematic uncertainty in the determination of the atmospheric parameters that describe the aerosol distribution (HAL and VAOD). We have compared the atmospheric database used in this

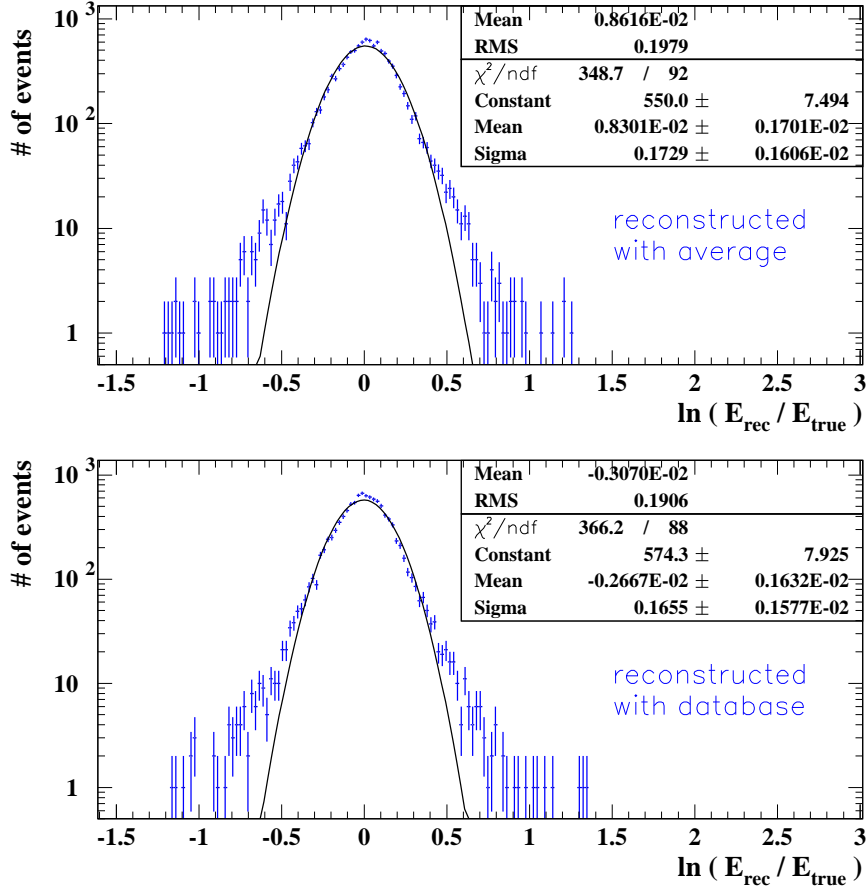


Fig. 14. The energy resolution is shown as the natural logarithm of the ratio of reconstructed over true (input) energy. The top panel shows the resolution in a MC set generated using the atmospheric database and reconstructed with seasonally averaged atmospheric parameters. For the ratio of reconstructed over true energy (not its logarithm) one obtains a width of 21.9% (RMS) and a  $\sigma$  of the Gaussian fit of 18.9%. The bottom panel shows the resolution in the same MC set when analyzed using the database. The RMS width and  $\sigma$  of the ratio are 21.0% and 18.0%, respectively.

study with an independent result from an analysis of laser shots with different geometries, which were reconstructed with independently developed software. The reconstructed energies one obtains with this independent database are on the average 5% lower than the values presented here. The average difference remains smaller than 7% at the highest energies.



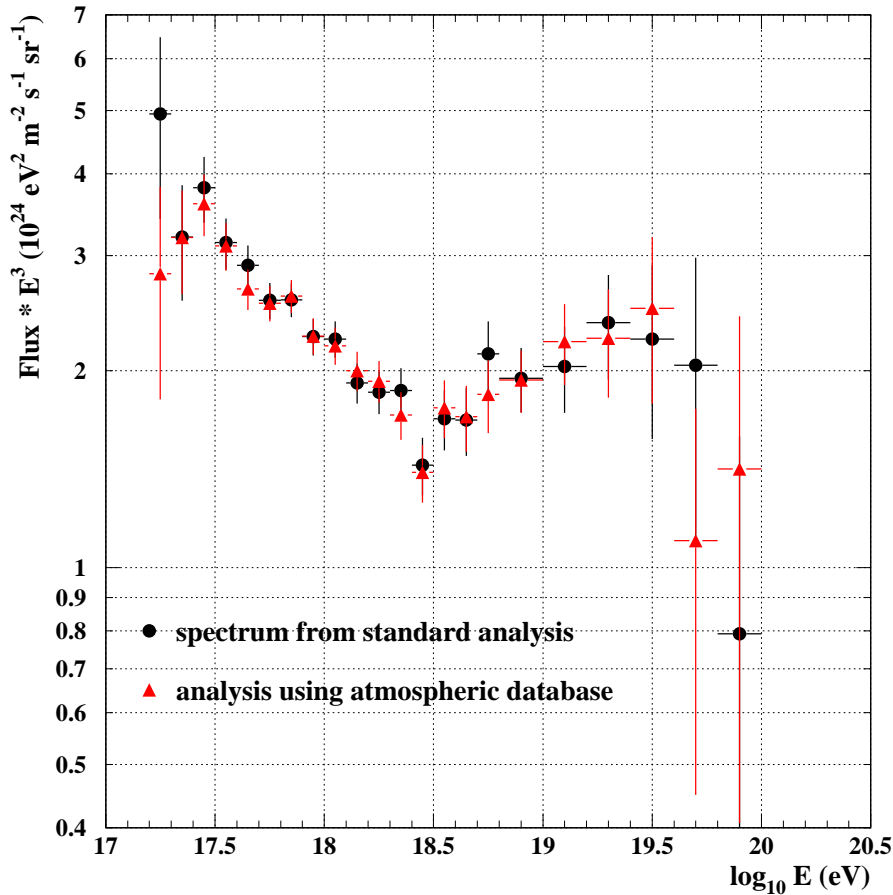


Fig. 15. The HiRes-II spectrum from our standard analysis is shown in circles. The spectrum resulting from an analysis that was using the atmospheric database in the determination of the aperture and in the reconstruction of the data is shown in triangles.

## 6 Conclusions

None of the sources of possible systematic uncertainties we have studied here contribute significantly to our published estimate of the systematic uncertainty. The bias introduced by using an  $E^{-3}$  power law instead of a more realistic spectral shape is not very significant in the “ankle” region. Our calculated aperture is sensitive to the assumed input composition for energies below  $\sim 10^{18}$  eV for HiRes-II. By using a measured composition as an input to our simulation programs, our analysis does not depend on the assumed hadronic interaction model. For the 17 month period tested here, the description of the aerosol density using an hourly database does not cause any significant differences in the spectrum, when compared with an average atmosphere. We also found no significant changes in the reconstructed energies for the time period under study.

## Acknowledgements

This work is supported by US NSF grants PHY-9321949, PHY-9322298, PHY-9904048, PHY-9974537, PHY-0098826, PHY-0140688, PHY-0245428, PHY-0305516, PHY-030098, and by the DOE grant FG03-92ER40732. We gratefully acknowledge the contributions from the technical staffs of our home institutions. The cooperation of Colonels E. Fischer and G. Harter, the US Army, and the Dugway Proving Ground staff is greatly appreciated.

## References

- [1] T. Abu-Zayyad *et al.*, Proceedings of the 26th International Cosmic Ray Conference **5**, 349 (1999)
- [2] J. Boyer, B. Knapp, E. Mannel and M. Seman, Nucl. Inst. and Meth. **A 482**, 457 (2002)
- [3] K. Greisen, Phys. Rev. Lett. **16**, 748 (1966).
- [4] G.T. Zatsepin and V.A. K'uzmin, Pis'ma Zh. Eksp. Teor. Fiz. **4**, 114 (166) [JETP Lett. **4**, 78 (1966)].
- [5] R. U. Abbasi *et al.*, Phys. Lett. B **619**, 271 (2005), astro-ph/0501317
- [6] R. U. Abbasi *et al.*, Phys. Rev. Lett. **92**, 151101 (2004), astro-ph/0208243
- [7] D. Heck, J. Knapp, J. N. Capdevielle, G. Schatz and T. Thouw, FZKA 6019 (1998), Forschungszentrum Karlsruhe, [http://www-ik3.fzk.de/~heck/corsika/physics\\_description/corsika\\_phys.html](http://www-ik3.fzk.de/~heck/corsika/physics_description/corsika_phys.html)
- [8] N. N. Kalmykov, S. S. Ostapchenko and A. I. Pavlov, Nucl. Phys. B (Proc. Suppl.) **52B**, 17 (1997)
- [9] R. U. Abbasi *et al.*, Astropart. Phys. **23**, 157 (2005), astro-ph/0208301
- [10] R. S. Fletcher, T. K. Gaisser, P. Lipari and T. Stanev, Phys. Rev. D, **50**, 5710 (1994)
- [11] R. U. Abbasi *et al.*, Astropart. Phys. **25**, 74 (2006)
- [12] G. Cowan, Statistical Data Analysis, Oxford Science Publications, 1998
- [13] D. J. Bird *et al.*, Phys. Rev. Lett. **71**, 3401 (1993)
- [14] T. K. Gaisser and A. M. Hillas, Proceedings of the 15th International Cosmic Ray Conference, **8**, 353 (1977)
- [15] C. Song *et al.*, Astropart. Phys. **14**, 7 (2000), astro-ph/9910195
- [16] W. R. Nelson, H. Hirayama and D. W. O. Rogers, SLAC Report, **265** (1985)

- [17] D. Heck, M. Risse and J. Knapp, Nucl. Phys. B (Proc. Suppl.) **122**, 364 (2003)
- [18] S. S. Ostapchenko, presentation at the VIHROS CORSIKA school 2005 in Lauterbad, Germany
- [19] T. Abu-Zayyad *et al.*, Astrophys. J. **557**, 686 (2001), astro-ph/0010652
- [20] T. Abu-Zayyad *et al.*, Phys. Rev. Lett. **84**, 4276 (2000)
- [21] R. U. Abbasi *et al.*, Astrophys. J. **622**, (2005) 910-926
- [22] Y.Fedorova (HiRes Collaboration), Proc. of the 29th Int. Cosmic Ray Conf. (2005)
- [23] D. J . Bird *et al.*, Ap. J. **424**, 491 (1994)
- [24] T. Abu-Zayyad *et al.*, P.R.L. **84**, 4276 (2000)
- [25] N. Nagano *et al.*, J. Phys. G **18**, 423 (1992)
- [26] M. I. Pravdin *et al.*, Proc. 26th ICRC, Salt Lake City (1999).
- [27] R. U. Abbasi *et al.*, Astropart. Phys. **25**, 93 (2006)